JOURNAL OF SPACECRAFT AND ROCKETS
Vol. 42, No. 4, July–August 2005

Fabrication and Operation of Microfabricated Emitters as Components for a Colloid Thruster

John Stark*
University of London, London, England E1 4NS, United Kingdom
Bob Stevens†
Rutherford Appleton Laboratory, England OX11 0QX, United Kingdom
Matthew Alexander‡
University of London, London, England E1 4NS, United Kingdom
and
Barry Kent§
Rutherford Appleton Laboratory, England OX11 0QX, United Kingdom

An integrated design for a colloid thruster, using microfabricated components, is described. This thruster is suitable as a propulsion unit for both a small satellite and a conventional satellite. One key component of the thruster is a nano-emitter array. A description of the fabrication processes that are used for the manufacture of these nano-emitters is provided. We report the first quantitative results for the electrospray current as a function of both flow rate and applied voltage for these emitters. Electrospray test results comparing the performance of these new emitters with conventional stainless-steel capillaries reveal that when allowance is made for the electrostatic configuration differences the spray current demonstrates qualitatively similar flow-rate dependence. Importantly, our electrospray current measurements from differently sized emitters show, for the first time, that this current is sensitive to the geometry of the emitter itself. This result is used to highlight the role of emitter design in the efficiency of a colloid thruster.

Introduction

THE concept of colloid propulsion is not new. Early work on such concepts can be traced to the early 1960s (Refs. 1–3) when a variety of studies and significant developments were undertaken in both Europe and the United States. There are many desirable features of colloid thrusters, not the least of these being the very modest power per unit thrust inherent in such devices. Although this performance comes typically at the cost of lower specific impulse relative to other electrostatic propulsion systems including ion (Kaufmann engines)[4] and field emission devices,[5] the high efficiency of colloid systems continued to attract funding well into the 1970s (Ref. 6). Development of working thrusters suffered and generally failed, however, principally as a result of a poor technical understanding of the physical elements underlying the electrospray process and hence control of critical parameters including the charge to mass ratio of sprayed droplets. Improved understanding however followed from the work led by Fenn's group at Yale[7] during the 1980s and de la Mora and Loscertales work[8] during the early 1990s. Their research followed the identification and subsequent development and use of electrospray technology as a method of soft ionization for large biomolecules, such as proteins and enzymes for analysis by mass spectrometry. There is now a broad characterization of the relationships between stable flow rate, applied electric field, and the charge-to-mass ratio q/m of electrospray charged droplets, although these relationships are principally derived from data for electrospray systems operating into a gas at atmospheric pressure.

The improved understanding has resulted during the past few years in development of a conventionally fabricated colloid thruster led by Busek,[9] with a thruster designed to fly on the Smart 2 mission. For this thruster development the requirements have been principally focused on the ability to achieve ultrafine thrust control, in order potentially to satisfy missions such as LISA. Our own approach has been rather different however in that we are additionally interested in the propulsion issues related to small satellites. There are therefore two additional developments that have facilitated our own work in looking again at colloid thruster operation: 1) an interest and commitment to the development of small satellites and 2) the development of microfabrication techniques. The former has provided a stimulus to develop miniaturized components, whether or not the application is to small satellites. The latter provides the potential capability for a technology to realize the full potential of colloid systems. The nexus of these two features has thus led to a collaborative program between Queen Mary, University of London, and the Rutherford Appleton Laboratory. This program has the goal of developing a fully integrated microfabricated colloid thruster.

The key elements of a colloid thruster are shown schematically in Fig. 1. An emitter, most frequently in the form of a capillary, is used to supply a conductive fluid into a region of an intense electric field, typically of order 10^5–10^7 V/m. As observed originally by Zeleny[10] and subsequently characterized by Taylor,[11] a balance between fluidic forces associated with surface tension and any applied static pressure, with the electric stress exerted on the fluid, results in a stable Taylor cone. Increased electric stress results in the formation of a stable jet under certain conditions. This jet eventually breaks up into a stream of charged droplets. In a colloid propulsion system these droplets are further accelerated in the electric field, leading to potential momentum exchange and hence the production of thrust. A working fluid is stored in a reservoir, or propellant tank; this tank then supplies fluid via an appropriate low-loss pipe line to the emitter. As in all electrostatic thrust devices, the charged beam must be electrically neutralized, and some method is therefore required

Presented as Paper 2003-4852 at the 39th Joint Propulsion Conference, Huntsville, AL, 20–23 July 2003; received 12 January 2004; revision received 28 July 2004; accepted for publication 4 August 2004.

*Head of Department, Department of Engineering, Queen Mary.
†Process Technology Group Leader, Central Microstructures Facility.
‡Postdoctoral Researcher, Department of Engineering, Queen Mary.
§Head of Applied Physics Group, Space Science and Technology Department.

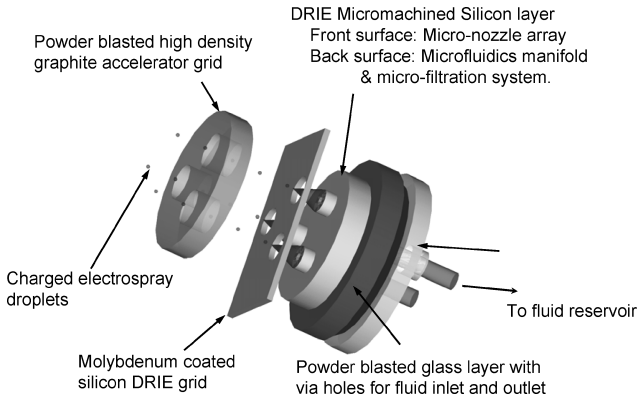

Fig. 1 Microfabricated colloid thruster layout, neutralizer not shown.

to supply oppositely charged species into the plume. Most concepts result in a positive charge on the droplets, requiring electron injection to the plume to achieve neutralization. Perel et al.[3] noted however that the electrospray process operates in a similar manner independently of the relative field direction between the emitter and grid: a positive emitter potential relative to an "accelerator" electrode yields a positive droplet stream, whereas a negative potential results in negatively charged droplets. Thus in a colloid thruster it might be possible to remove the need for a neutralizer either by having multiple emitters, some of which are positive and some negative, or alternatively by application of a fluctuating potential applied to the emitter, again resulting in a net charge balance with the spacecraft.

Differing thruster concepts arise from the way in which these key components are utilized and realized. Historically all development focused upon the use of individual capillary structures fabricated into an array, with discrete components used for propellant storage, supply and control, accelerator grid(s), and neutralization. Additionally the size of the capillary used in older concepts tended to be rather large, and not necessarily linked to the anticipated flow rate through the emitter. The electrohydrodynamic conditions thus created in these early designs did not necessarily produce good thrust stability because multiple Taylor-cone structures on a single capillary could arise.

While noting that there are two distinct themes in the current resurgence of interest in colloid propulsion systems, most of the published results focus upon configurations with discrete elements in the thruster. Thus collaborative work reported from the Massachusetts Institute of Technology (MIT)[12] in association with Yale and Busek,[9] has led to the development of a thruster that contains 57 individual stainless-steel emitters brazed into a supporting structure. These emitters are quite long, 1 cm, and have an internal diameter of 30 μm. The propellant is highly doped formamide, with a conductivity of 0.5 S/m. The work at Stanford has a larger array of 100 hypodermic needles, with doped glycerol as the propellant.[13]

Reports on colloid thruster designs that have adopted microfabrication techniques are limited. In the main these reports have provided a description of concepts, rather than any evaluation of electrospray properties. Workers at MIT have microfabricated a design[14] that consists of an hydraulic system of fuel tanks, manifolds, and an array of 20 emitters fabricated in the silicon wafer plane. Each emitter has a 12-μm-square internal profile and a length of 15 mm. These emitters provide a high hydraulic resistance so that flow can be controlled via tank head pressure. Nickel electrodes fabricated on an insulating dielectric wafer start the electrospray (and liquid flow). This electrode system is attached and aligned to the hydraulic component via a clip mechanism. More recently the MIT group has looked at larger arrays, where the emitting elements are externally wetted by the liquid under test.[15] Another group microfabricated 3-μm-diam emitters, with low hydraulic resistance, in the surface of a silicon wafer.[16] Extraction was to be performed by electrodes insulated from the silicon by a SiO_2 film, but prototypes failed because of premature insulator breakdown. Later insulators routinely held 3 kV in poor vacuums with small electrode separations, but no sprays were obtained.

In this paper we report for the first time results that we have obtained from microfabricated emitters in which, unlike the early work on colloid thrusters in the 1960s, each emitter supports a single Taylor-cone-jet structure. To develop a useful colloid engine, it is now essential to manufacture arrays of emitters because flow through a stable cone-jet mode electrospray can only be maintained at low flow rate. The actual value for flow rate at which stable operation is achieved is dependent upon the conductivity of the liquid used for electrospray.[8] As an example, a liquid having the appropriate characteristics for a colloid thruster requires high conductivity, and the minimum stable flow rate for such a liquid is of order 0.1 nl/s. The thrust then developed from the spray from this single Taylor cone with such a liquid would only be of order 0.1 μN. This clearly identifies the need for a significant number of individual emitters if a useful level of thrust is to be obtained, making the colloid emitter a suitable device applicable to space missions.

The emitter is, however, only one of the elements of a thruster system. A microfabricated emitter is ideally suited as part of an integrated microfabricated colloid thruster. This thruster requires a number of key components including not only the emitter array, but also a propellant feed system, a propellant reservoir, and two electrostatic grids with the first of these grids being used to establish the electrospray process itself and the second to accelerate the charged droplets to an appropriate velocity in a directed beam. One concept for such an integrated thruster is presented by Stark et al.[17]

In this paper we focus on two issues relevant to our development program directed to an integrated colloid thruster: the fabrication process of silicon nano-emitters and evaluation of spray properties from these nano-emitters. Both individual emitters and arrays of emitters have been fabricated. We compare here the electrospray properties of these emitters with those sprays formed from conventional stainless-steel emitters.

Benefits of Silicon Microfabrication

There is an established supply chain of materials, equipment, and trained manpower for silicon-based microelectromechanical systems foundry services. Deep reactive ion etch (DRIE) systems, which use the patented Bosch or Advanced Silicon Etch (ASE)^{TM} process, for anisotropic etching of silicon are established with Alcatel, Trikon, Surface Technology Systems (STS), and Oxford Plasma Technology being leading equipment manufacturers. Current commercial systems can etch 200-mm-diam silicon wafers. The STS multiplex inductively coupled plasma (ICP) used for the emitter fabrication process was set up to process 100-mm-diam silicon using the ASE process. This process would be capable of producing silicon emitters with aspect ratios up to 10:1 after rigorous process optimisation. Typically a 50-μm outer diameter emitter could be produced with a height of 500 μm. Established photolithographic in-contact masks can be used to define features with critical dimensions that are less than 1 μm. Deposition of high-quality dielectrics and metallic thin films use techniques, which have been developed for the silicon microelectronics industries, namely, physical and chemical vapor deposition systems. Access to these equipments enables reproducible emitter arrays to be manufactured from silicon wafers.

Conventional electrospraying within colloid thrusters is obtained from metallic emitters. The use of pure silicon for the emitter does therefore have limitations in that there is a requirement to provide at least a surface of material that can conduct electrons to or from the sprayed fluid. Possible solutions to this problem are to either provide a conductive film surface over the silicon by an appropriate deposition process or by highly doping the silicon to create a conductive silicon material. Care must be taken in the use of conductive coatings to ensure that the coating is sufficiently stable to withstand the electrochemical corrosion processes occurring between the liquid and the emitter. If doping is adopted, then it is necessary to consider whether the spray is operated in positive or negative mode. The configuration that we have adopted is with a positive potential

applied to the emitter, resulting in positively charged droplets. The formation of these requires electron loss at the emitter. This can be obtained therefore by doping the silicon to create a p-type material. Sufficiently highly doped silicon leads to degeneracy, in which case the silicon material can be used to either inject or remove electrons from the liquid. For the spray liquid used in this paper, we have however identified a further limitation in that the liquid easily wets the silicon surface. For a large array of such emitters, there is then the potential for flooding the emitters with liquid. As a result, in this paper we have used a conductive film to provide electrical connection, although the silicon is doped to achieve high conductivity.

Emitter Layer Fabrication Process

The fabrication sequence described here facilitates manufacture of single emitter and wafer-level multiple emitter arrays. The starting material was 100-mm-diam, 1-mm-thick N-type 1-10 Ohm-cm, double-side polished silicon wafers. The first step was to deposit 4-μm-thick layers of silicon dioxide on to both sides (sides 1 and 2) by wet thermal oxidation. An additional 2-μm layer of silicon dioxide was then deposited on side 1 of the wafer by plasma enhanced chemical vapor deposition.

Following the deposition of the adhesive promoter hexamethyldisilizane (HMDS) onto side 1, this surface was coated with 10 μm of AZ4562 photoresist, by dispensing 250 μl of AZ4562 into the center of the wafer and then spin coating at 1400 rpm for 28 s, with an acceleration of 500 rpm $\cdot$ s^{-1}. The layer was baked for 10 min on a hot plate at 90°C. Hard-contact ultraviolet (UV) exposure through a chrome on borosilicate glass mask was used to photodefine the AZ4562 resist. The broadband UV dose was generated by a high-pressure mercury vapor lamp; the dose conditions adopted were an exposure time of 25 s with an illumination intensity of 10 mWcm^{-2}. The exposed photoresist layer was then developed in a tank of aqueous developer solution for 5 min, which ensured that all the exposed resist was removed. The layer was then rinsed in a weir wash with deionized water for 3 min and then spin dried under a nitrogen gas stream at 2000 rpm for 80 s. The wafer was subjected to an oxygen plasma descum, for 2 min using a parallel-plate reactive ion etching systems (Oxford Plasma Technology, RIE80 plus). The process conditions were an rf power of 300 W at a pressure of 100 mtorr, and an oxygen flow rate of 100 sccm.

After descum, the wafers were loaded into a parallel-plate reactive ion etch system. The 6 μm of silicon dioxide was etched using an argon (7 sccm) and CHF_3 (21 sccm) plasma at 250 W and a pressure of 30 mtorr. The etch time was 6 h. The remaining AZ4562 resist layer was ashed in an oxygen plasma. The etched oxide surface was then protected from possible surface damage by spin coating PI 2771 polyimide and baking at 300°C for 30 min on a hot plate. The oxide layer on side 2 was then prepared for patterning by an aggressive oxygen plasma clean and then deposition of HMDS. The process steps similar to those just described were used to define the oxide etch mask on side 2. The resulting cross section after 31 processing steps is shown in Fig. 2.

After oxide mask definition the wafer was immersed in EKC265 for 1 h at 70°C to remove all organic layers from sides 1 and 2. The wafer was then rinsed and dried. A 100-mm-diam silicon carrier wafer was then coated with "cool grease," which has high thermal

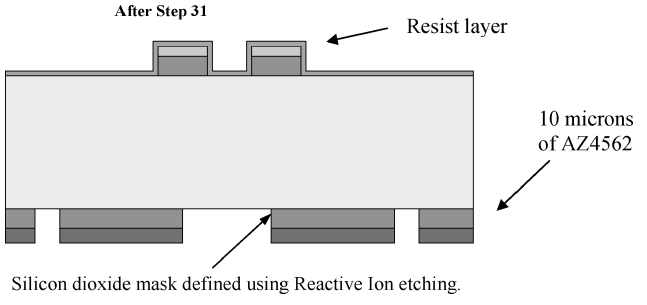

Fig. 2 Processed chip after 31 process steps.

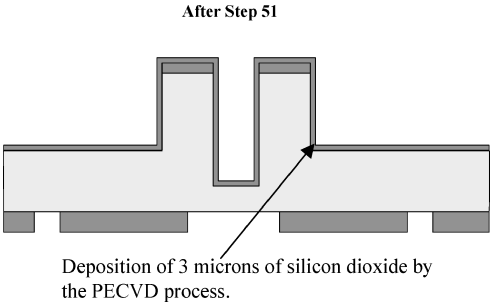

Fig. 3 Processed chip after 51 process steps.

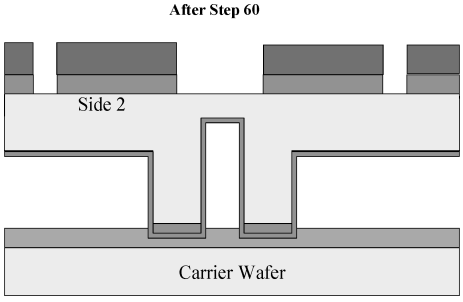

Fig. 4 Processed chip after 60 process steps.

conductivity. Side 2 of the device wafer is then bonded to the greased surface of the carrier wafer by placing on a hot plate at 90°C for 5 min. Side 1 of the wafer sandwich is descummed in an oxygen plasma, and then a photoresist layer of AZ4562 is coated, and the aligned in-contact mask is defined by standard photolithographic techniques. The descummed surface is then loaded into a surface technology systems inductively coupled plasma Reactive Ion etcher with the capability to run an ASE, which uses SF_6 as the silicon etch process and C_4F_8 as the passivation gas. The first process is to produce a 5-μm undercut of the in-contact mask, which enhances the aspect ratio of the subsequent anisotropic silicon DRIE etch, which defines the through-wafer capillaries. The isotropic etch uses an ICP coil power of 500 W with a platen power of 20 W. The total etch time was 2.5 min. The capillary etch is then performed by using the cycling ASE process. There are two repeating cycles for the etch process. The etch cycle lasts for 12 s and uses SF_6 at a flow rate of 135 sccm, with the automatic pressure controller in manual mode at 82%. The ICP coil was run at 800 W and the platen power at 20 W. Following the etch cycle, the machine automatically switches to the passivation cycle. The passivation conditions were an ICP coil power of 600 W and 0 W platen power for a time of 8 s. The total number of cycles was 720, which results in a etch depth of over 500 μm. The etched wafer is then unloaded, and the remaining resist layer removed by reactive ion etching. The wafer sandwich is then loaded into the ICP deep RIE where it is etched for 540 cycles to remove 400 μm of silicon. This leaves a structure shown in Fig. 3. Following the etch to define the outside of the emitter and to extend the depth of the emitter capillary, the carrier wafer is debonded from the device wafer. Side 2 is cleaned using iso propyl alcohol to remove the majority of the cool grease. The wafer is then immersed in EKC265 for 1 h to remove any remaining organics. The wafer is rinsed and dried before loading into an Oxford Plasma Technology DP800 plasma-enhanced chemical vapor deposition system. The process conditions were SiH_4 (100 sccm) and N_2O (50 sccm), platen temperature of 300C, rf power of 15 W, and a process time of 142 min. This deposits a conformal coating of silicon dioxide, which is 2 μm thick, on side 1 of the wafer surface. The wafer is bonded to a new carrier wafer with side 1 facing the cool grease surface. The wafer is then descummed, before loading into the ICP deep RIE. A modified silicon etch process is used to expose the emitter capillary as shown in Fig. 4, at this stage the wafer having been subject to a total of 60 processing steps. Then after all capillaries

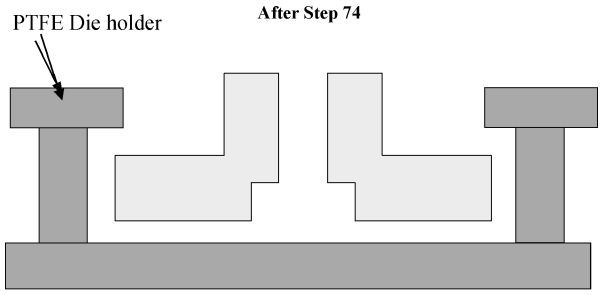

Fig. 5 Processed chip after 74 process steps.

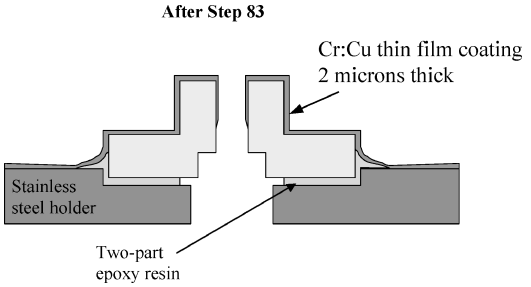

Fig. 6 Processed chip after 83 process steps.

have been uncovered, a photoresist is painted onto the etched recess to prevent further etching in the capillary regions. However the DRIE is continued to etch through the wafer to define the circular die with single or multiple emitter arrays. The die are then demounted from the carrier wafer using a vacuum pen and rinsed in isopropyl alcohol and EKC265. Following the removal of organic materials, the die is placed in a PTFE holder before oxide strip using 7:1 deionized water: hydrofluoric acid. The resulting structure is shown in Fig. 5. The emitter die was rinsed and dried prior to mounting onto a stainless-steel ring using a two-part epoxy adhesive. The epoxy is cured in an oven at 90°C for 1 h. The assembly is loaded into dc magnetron sputtering system, where a chromium thin film of 0.1 μm is deposited followed by a copper layer of 2 μm. The emitter subassembly after 83 processing steps is shown in Fig. 6. Following this step, the devices were assembled into the colloidal thruster test rig.

Fabrication Results

The process allows single emitters to be fabricated with minimum dimensions of 35 μm outer diameter, with a 25-μm inner diameter. A variety of emitter lengths have been fabricated, ranging from 15 μm height to 400 μm.

The same process can produce clusters of emitters, with a varying number of emitters and pitch between emitters. Figure 7 shows a 100-mm-diam wafer with 55 electrospray heads. Each head has a cluster of emitters at the centre of the 10-mm-diam die. The numbers of emitters per cluster range are either 3,7, or 19. Their layout is in the form of a triangular array. Figure 8 shows a plan view of a cluster with seven emitters.

Fabricating emitter arrays at the wafer scale can produce colloidal thrusters with large thrust per unit area. As an example, a 100-mm-diam wafer with 20,000 emitters was defined within a 75-mm-diam area. Figure 9 shows a plan view of a number of the emitters within this wafer, showing a uniform spatial distribution of emitters. Thrust from this density of emitters is expected to be on the order of 1 mN/cm^2.

Electrospray Properties of Nano-Emitters

Performance data for the microfabricated emitters were obtained in an experimental rig described in greater detail elsewhere.[18]

Fig. 7 Processed wafer containing 55 separate emitter arrays.

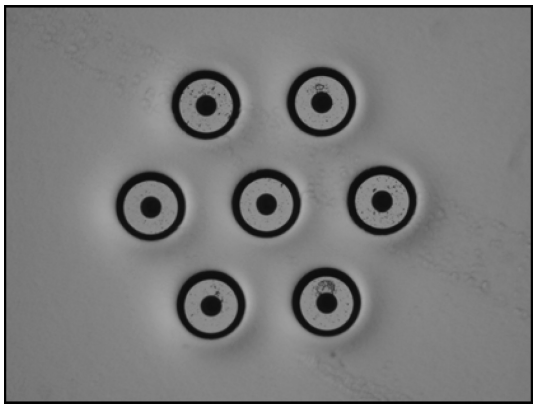

Fig. 8 Detailed image of an array containing seven emitters, each of external diameter 400 μm.

Briefly, this setup is shown in Fig. 10. Particular attention in designing this rig was paid to the need to make online flow-rate measurements. For these we adapted a standard approach, namely, the measurement of a pressure drop along a specific flow pipe, albeit in a particularly demanding setting. The flow pipe was a custom-built inert glass-lined tubing (GLT)^{TM} from SGE, Ltd. The tubing has an internal diameter of 0.3 mm and a length between pressure tapings of 100 mm. The pressure at each tapping is measured by one of a pair of Digiquartz Model 740-23A temperature compensated quartz crystal pressure transducers. These have an accuracy of one part in 10^6. The electrospray test fluid does not come into direct contact with the active sensor head, but is separated by a buffer oil. To obtain accurate flow data, it is essential to ensure that the interface between these two liquids is gas free, a process which proves to be particularly demanding to achieve, because the narrow bore tubing is required to be evacuated. Following filling the system, the flow system is calibrated by collecting a sample of test liquid over a defined time period. The accuracy of this approach achieves an absolute calibration of 1 nl/s (Ref. 18). The electrospray measurements were obtained with the nano-emitter having high positive voltage applied. This method thus also requires that the transducers were isolated from ground potential.

The required electrostatic field at the emitter to achieve a stable Taylor-cone-jet structure was obtained by placing a stainless-steel aperture some 4 mm away from the backplane of the emitter. The aperture used was circular and had a diameter of 1 cm and was optically centered on the axis of the emitter. Spray current passing through the aperture was measured using a Faraday cup placed 5 cm downstream of the aperture. Automatic logging of currents on both the aperture, referred to here as the grid current, and the emitter was achieved online, using opto-isolation. These currents were measured by a custom-built ammeter, which comprised a two-stage optically isolated system to transmit safely a signal from high

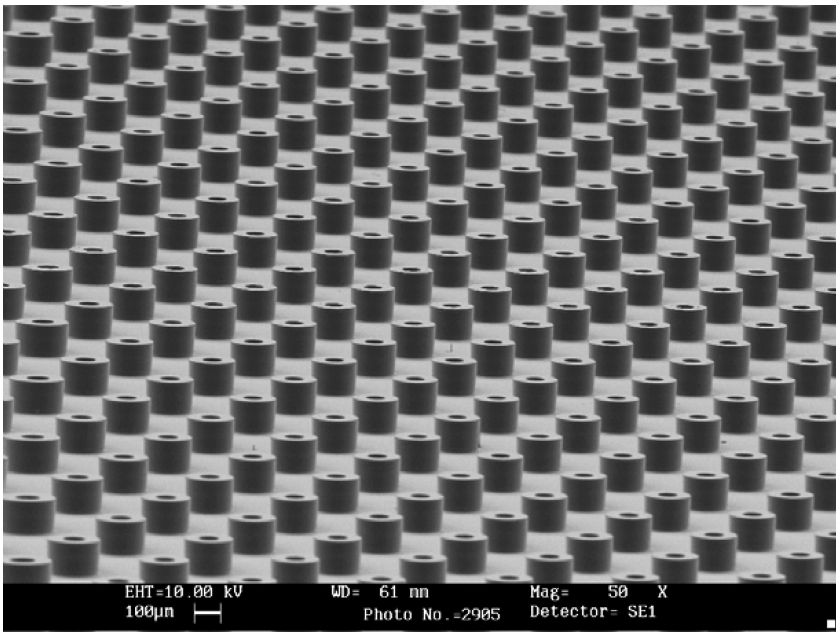

Fig. 9 Image of part of an array containing 20,000 emitters, within 100 mm diam.

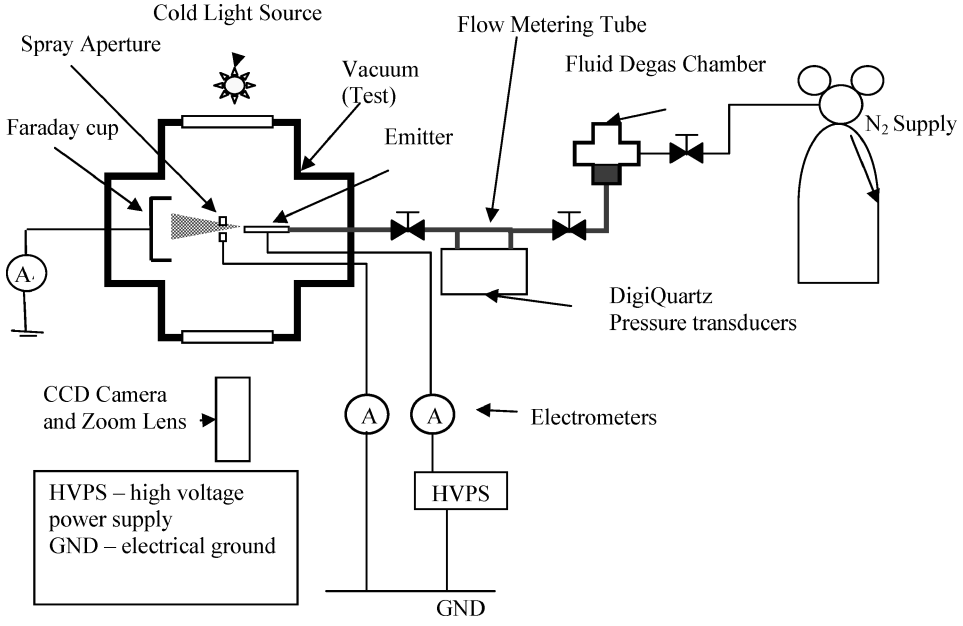

Fig. 10 Schematic of experimental configuration.

voltage to a data logger at ground potential. A battery-powered high-voltage stage, floated at the same potential as the emitter, contains a current-to-voltage converter in the transresistance configuration. This was designed to measure currents up to $\pm 2\ \mu$A with a response of $\sim$1 mV/nA and a time response of 1 s. This converter is followed by a voltage-to-frequency converter for optical signal transmission. The AD650 V to f chip was configured for bipolar inputs, giving 50–150 kHz for an input range of ± 2.5 V. A fiber-optic cable connected to a frequency-to-voltage converter chip at ground potential comprises the second stage, which is then directly and safely connected to a PC. Such isolation is clearly required on the high-voltage line, but was also included on the grid current monitor in order to protect instrumentation from the potential for short circuit to high voltage. In all cases reported here, current balance between emitter, grid, and Faraday cup was observed, with the current flow to the grid being typically less than 1% of the emitter current. The Faraday cup was directly connected to a Keithly Instruments pico-ammeter (type 486), which was not interfaced to the data-logging computer. As a result, we refer in the figures to the emitter current rather than the spray current itself.

The emitter current to voltage characteristics, for a single nano-emitter, at four flow rates are shown in Fig. 11. In these reported experiments we have not attempted to use a liquid suitable for a realistic propulsion unit. Instead the fluid used was triethylene glycol, doped with NaI in order to achieve a conductivity of 0.01 S/m. Our justification for this is that the liquid is inexpensive and is readily controllable while electrospraying under vacuum conditions. It also demonstrates negligible evaporation losses from the Taylor-cone structure. There is however one important handling issue regarding this liquid. Following preparation, it is important to maintain the solution in a dry nitrogen atmosphere, before further degassing in the fluid reservoir used to feed the electrospray emitter. This approach reduces the potential for water absorption, which has a significant influence on solution conductivity, and hence influences spray currents.

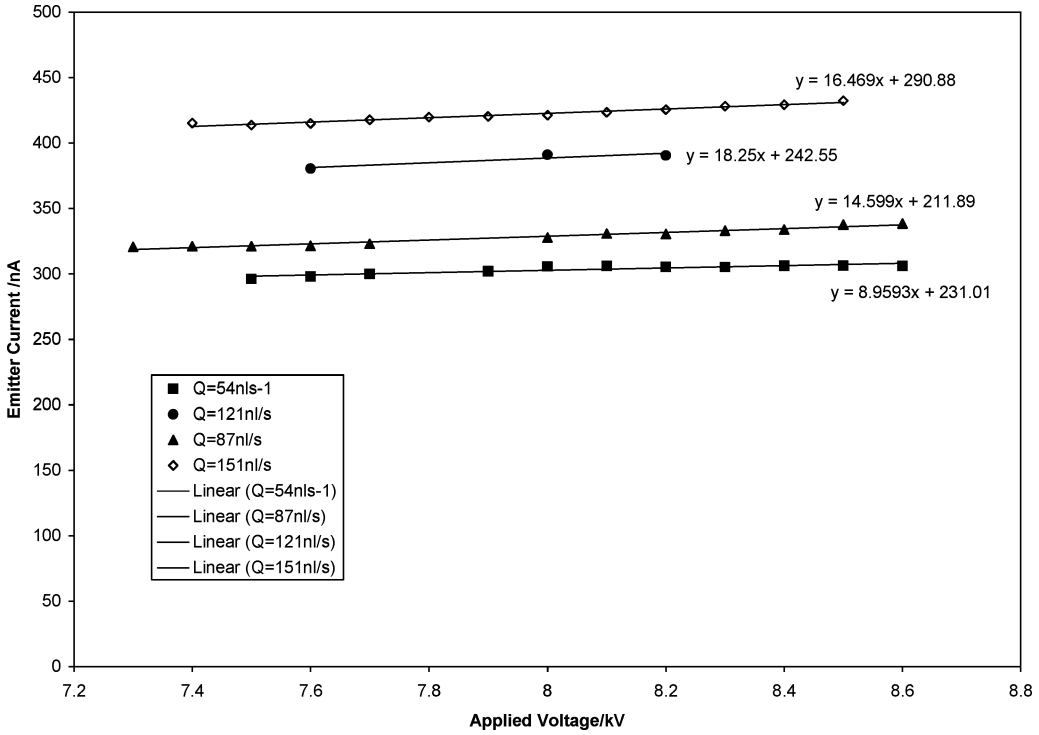

Fig. 11 Emitter current-voltage characteristic from single nano-emitter.

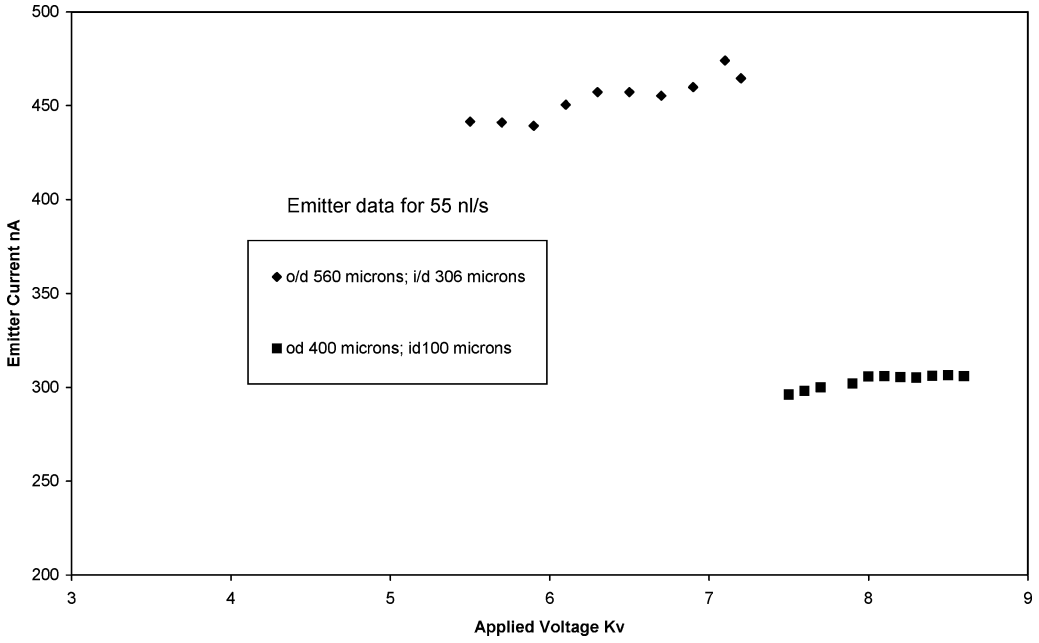

Fig. 12 Comparison of spray current for silicon nano-emitters with varying internal to external diameters at a flow rate of 55 nl/s.

The silicon emitter used to obtain the data in Fig. 11 had been coated in chromium/copper, and has an external diameter of 400 μm and internal diameter of 100 μm. The emitter is 400 μm long. This emitter was held in a specially manufactured holder. We observe from these data that the emitter current, and hence spray current, at a given flow rate is dependent upon the applied voltage. Because of the automated data-logging equipment used to obtain the data,[18] emitter current was measured to an accuracy of 2nA; typically long-term current fluctuations were less than 0.6%. Flow rates were measured absolutely to an accuracy of 1 nl/s, with relative flow measurements to 0.2 nl/s. As a result, the measurement uncertainties associated with the data presented in Fig. 11 are expected to be on the order of the size of the plotted points.

Figure 12 is a plot of the emitter current as a function of voltage at a single value of flow rate, 55 nl/s, again using the triethylene glycol solution having a conductivity of 0.01 S/m; here, however, we compare the emitter current for two different silicon nano-emitters. One of these is the same emitter as used in the collection of data plotted in Fig. 11: 400 μm outside diameter, with 100 μm internal diameter. The other emitter used has on outside diameter of 560 μm, with an internal diameter of 305 μm. It is apparent that there is a significant difference in the current observed, with typically the current from the larger emitter being on the order of 50 to 60% greater. This variation between emitters is not predicted by scaling law models generally adopted to identify electrospray properties[8,19]; these generally neglect the detailed electrostatic and physical conditions

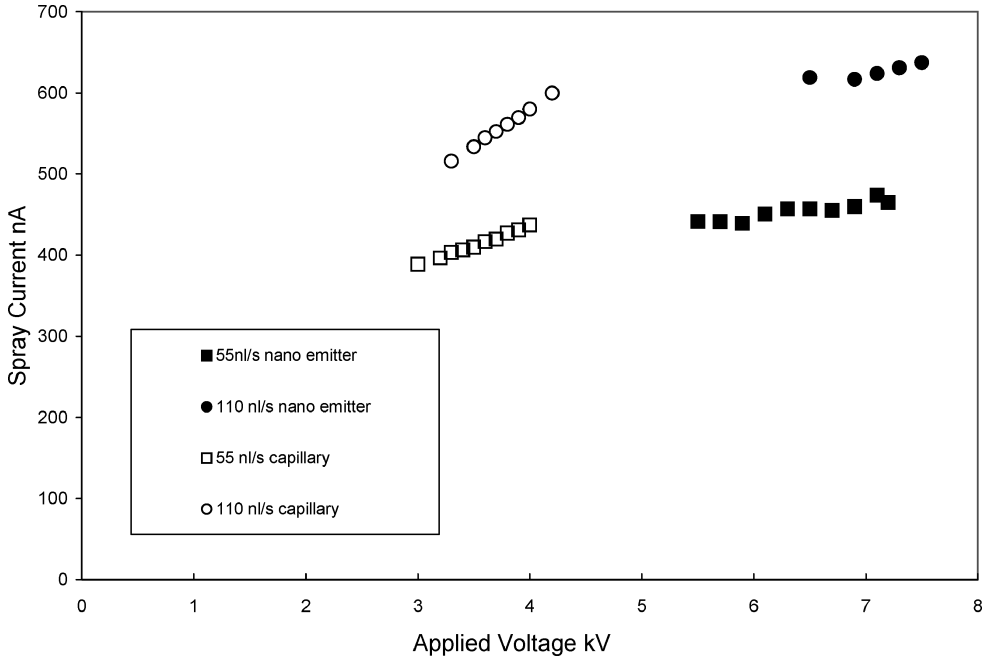

Fig. 13 Comparison of spray currents from stainless-steel capillary with silicon nano-emitter having the same internal and external diameters: length of capillary 13 cm and length of nano-emitter 400 μm.

of the capillary typically used in electrospray experiments. The increased current noted for the larger emitter is clearly suggestive of an increased area available for the oxidation reactions, that is, electrons being lost from the liquid, taking place at the emitter. Indeed if such reactions only take place at the upper surface of the emitter, then it is interesting to observe the ratio of areas for these two emitters is 1.47. However, it is simplistic to assume reactions solely taking place on this outer surface: the silicon used in the fabrication of the emitters has a reasonable conductivity, in the range 1–10 Ωcm, and hence the internal walls of the emitter would also be expected to contribute to the area available for reactions to take place. An additional complexity is that the chromium/copper coating was vacuum deposited, and hence there will, near the top surface on the inside of the emitter, be some rather thin layer of a higher conductivity membrane above the silicon structure. Although the larger bore emitter will have a larger area, for a given flow rate the fluid in the smaller bore will have a higher velocity. Given that charge transfer is taking place between the liquid and the emitter surface, a conventional electrochemical double layer will form close to the emitter surface in the liquid. The extent of this double layer formed can be affected by the fluid bulk flow rate, and this can therefore also influence reaction efficiency. These results demonstrate that if comparison is to be made between different emitters, geometric properties of these emitters must be controlled. This also identifies that investigation into the electrospray properties obtained from the microfabricated emitters in comparison with data from a conventional capillary electrospray is appropriate, because the metallic capillaries potentially provide a much larger area available for charge transfer at the liquid/solid interface.

One such comparison is presented in Fig. 13. The data in this figure were obtained using the same fluid as before with two flow rates: 55 and 110 nl/s, being shown. The emitter and capillary have the same values for internal and external diameters: 305 and 560 μm, respectively; however, the nano-emitter protrudes above the surrounding surface to only 400 μm, whereas the capillary extends to 13 mm above the surface on which it is mounted. Clearly it would be desirable to have identically sized capillary and emitter lengths for detailed data comparison, however, the standard ferrule fittings required to mount the conventional capillaries resulted in it being difficult to define the capillary height to an appropriate accuracy. It was deemed better to adopt a capillary length, which could be measured in such a way that the measurement uncertainties in this length would have a negligible influence on the overall aspect ratio of length to diameter because this parameter will clearly influence the operating voltage of the electrospray.

As anticipated, the data presented in Fig. 13 identify that a significantly higher voltage is required to operate in cone-jet mode for the emitter, although the spray currents demonstrate qualitatively similar values at the same flow rate. We presume that the higher voltage required can principally be ascribed to the different aspect ratios for the capillary and nano-emitter configurations, respectively. Let us assume initially that the dominant factor in defining the electric field for electrospray derives from the physical geometry of the emitter/counter electrode. This geometry then defines the field strength in the region of the emitter exit required to form the cone structure, with no protruding jet. Thus prior to electrospraying in cone-jet mode the fluid-vacuum interface is deformed by an electric field, whose magnitude is dependent upon the physical geometry, in like manner to that described by Smith.[20]

One method to try to collapse the data from the different configurations is by recognizing that at onset voltage, when a spray is first formed, the field strength in the region of the cone apex is anticipated to have a similar value for both the nano-emitter and the conventional capillary. The voltage at which this occurs in the two cases can then be used to normalize the voltage axis for the data. This process was undertaken, and the results are shown in Fig. 14. From this figure we can see more clearly that the magnitude and range of spray current data for the two configurations are similar, there appears however to be a difference both in the gradient and magnitude of the spray current, seen for both flow rates. These differences are rather greater than might be ascribed to the measurement uncertainties noted earlier, and it is important therefore to investigate what other features might explain the observations.

In Fig. 15 several images of the cone-jet structure are shown of the fluid cone-jet emanating from the nano-emitter and the capillary, at differing applied voltages but all at the same flow rate. These figures reveal that the shape of the cone itself is rather different, most notably in the extended nature of the cone observed for the nano-emitter configuration. For these data, the cone itself forms from an elongated fluid structure, not too dissimilar from the "silver bullet" mode noted by Chen et al.[21] In their data, however, the elongated structure was very sensitive to voltage, which was only obtained as the voltage was raised gradually. This mode is conventionally associated with applied voltages near to onset; however, here we

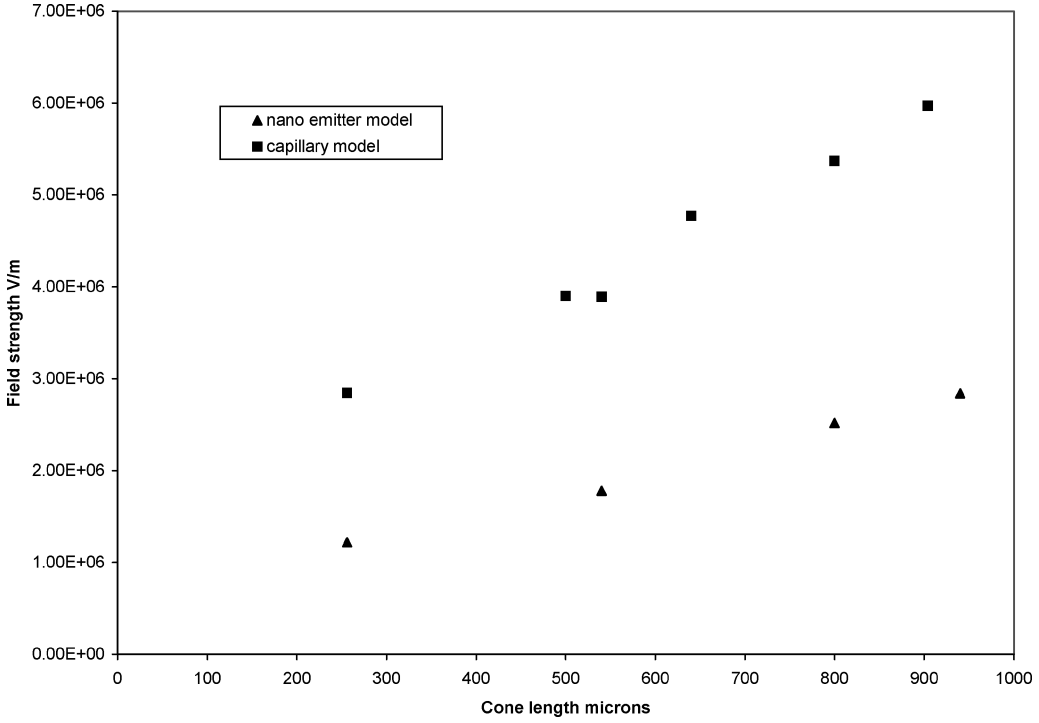

Fig. 14 Electrospray current voltage comparison with voltage normalized to onset voltage condition.

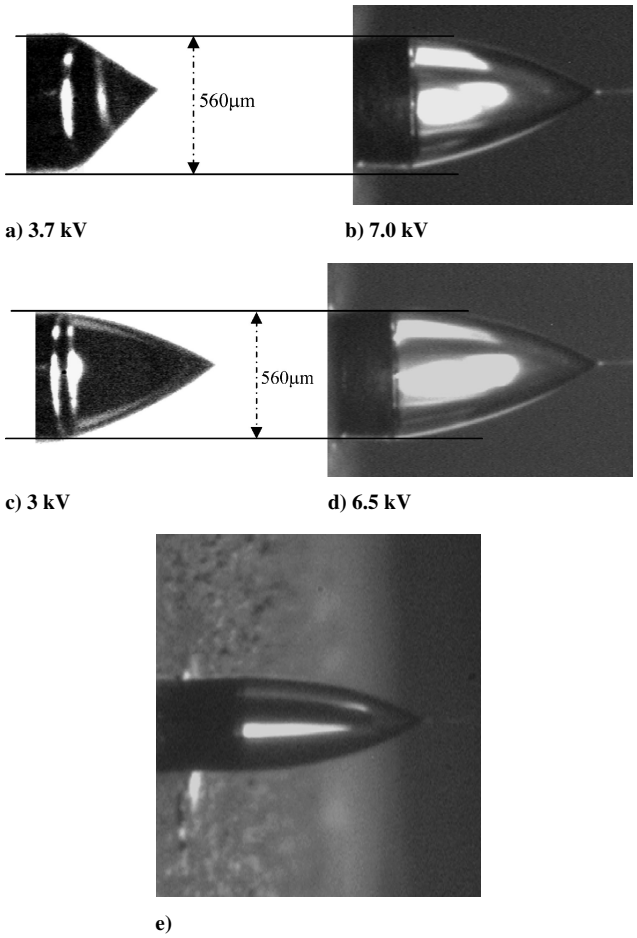

Fig. 15 Comparison of cone shape for a stainless-steel capillary (a and c) and for a 400-μm-long silicon nano-emitters (b and d) at varying voltages for a constant flow rate of 55 n/s; e) nano-emitter of 250 μm length showing the longer cone structure (see text for details).

have observed that the elongated mode extends through much of the stable electrospray range. Indeed, it is very difficult in these nanoemitters to form the conventional sharp Taylor-cone attached to the emitter/capillary surface. We also show for comparison the cone jet formed from a shorter nano-emitter, whose length is only 250 μm above the surrounding surface. This shows the elongated structure even more clearly.

We have analyzed a range of images, similar to those shown in Fig. 15, for a single flow rate 55 nl/s as a function of applied voltage for both the capillary and nano-emitter data. The cone length as a function of voltage is plotted in Fig. 16. The first observation concerning the general trend portrayed in Fig. 16 is that as the voltage is increased the cone becomes shorter. This trend is well established in the literature. However, the direct comparison between emitter and capillary data reveals that not only is the cone length generally longer on the emitter than that observed for the capillary, but also the change in this length over the stable electrospray region with voltage at this one flow rate is much reduced in the nano-emitter case. The nano-emitter data are reasonably well represented with a linear trend (regression coefficient 0.98), whereas the capillary data are not at all well represented by a linear trend (regression coefficient 0.76). We are not here suggesting that this difference is caused by the material properties of the capillary and emitter, but rather that it is caused by the detailed structure of the electric field in the vicinity of the respective cone jets as a result of their relative proximity to the planar surface on which the emitters are mounted.

These observations make it clear that the spray properties are indeed sensitive to the electrostatic conditions when, as we are, operating well above the minimum stable flow rate condition. However, our specific interest is to determine whether the nature of the emitter material—in the test case here with a silicon emitter coated with a thin copper on chromium surface—performs differently to a stainless-steel capillary. We are, however, now faced with the evident difficulty in making this comparison directly, because it is clear that the applied voltage also affects in a different manner the actual structure of the cone itself in our test configuration, and that this can be misinterpreted as changes in efficiency because spray current at these flow rates, as in Fig. 11, is indeed sensitive to applied voltage. We have therefore attempted to characterize the electrostatic field itself in a more detailed manner, rather than by the simple rescaling

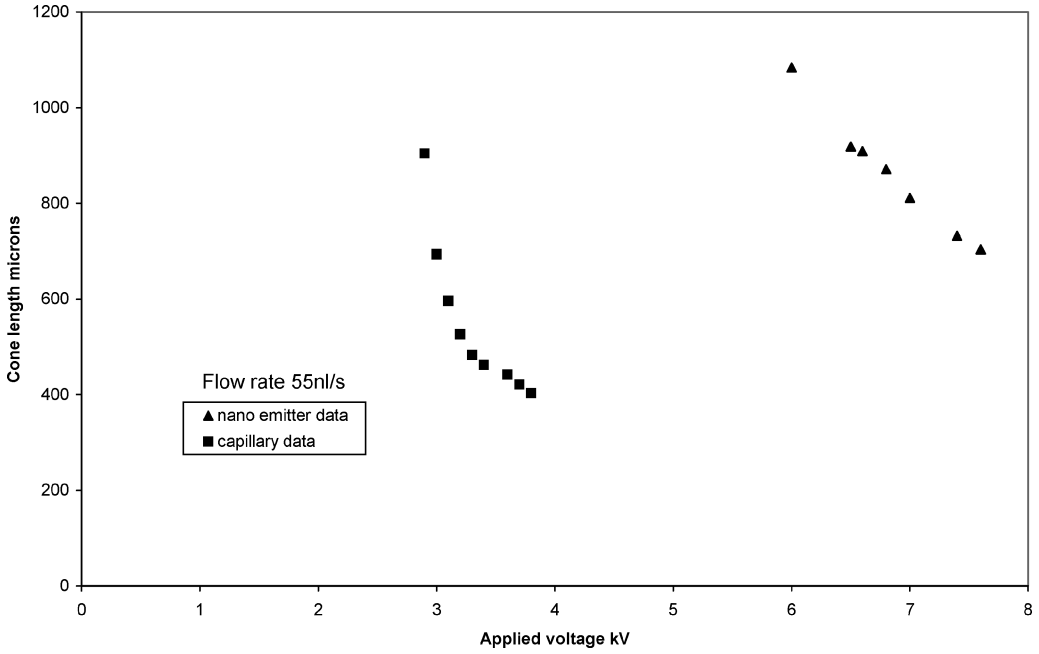

Fig. 16 Comparison of cone length as a function of applied voltage for silicon nano-emitter and stainless-steel capillary.

noted earlier. The electric field was therefore mapped using the software package Simion7. This package is not able to undertake detailed electrohydrodynamic simulation; however, we can make a simple first attempt at the field definition by using the observed images of Taylor-cone structures to define simulated electrode geometries within Simion7. These electrode surfaces are assumed within Simion7 to be perfectly conducting. This does not seem unreasonable, and indeed the assumption of a perfectly conducting cone is made in many of the papers published on electrospray properties, even though observations have been made which identify potential falls along the jet structure emanating from the cone.[22]

In each case evaluated, the separation between the emitter or capillary-electrode top surface and the counterelectrode was 4 mm, as in the experimental work. In the simulation the separation between adjacent nodes was 1.0 μm. A cone structure was then imposed on to this top surface with a length as observed in the images obtained. The back plane locations relevant for the emitter and for the capillary were set at the values noted for the experimental configuration.

One further simplification was made to perform the comparison for the electrostatic field configuration. For each simulation the cone structure was approximated to have a parabolic profile, with the radius of curvature at the apex constant, for all of the observed data recorded. This is clearly a simplification because it is recognized that as the cone forms the field in the apex region of the cone can change significantly. The critical reasoning for this assumption however is the following:

1) The camera used to observe the cone-jet structure is a PULNiX TM-1300 monochrome charge-coupled-device camera in conjunction with a Navitar 12:1 telescopic zoom lens. The overall horizontal and vertical resolution of the imaging system is 5 μm. If we make the not unreasonable assumption that the dimensions of the apex region are of order the size of the droplets formed during the spray breakup, following the model in Ref. 8 and using our measured properties of the triethylene glycol doped with NaI (Ref. 18), the expected droplet size is $\sim$0.1 μm at the minimum flow-rate condition. The experimental data were obtained significantly above minimum flow rate, but on the basis of the measured current dependence upon flow rate, and assuming that the droplets are fully charged to the Rayleigh limit, the derived droplet size is in the range 0.2 to 0.8 μm. It is therefore clear that the optical resolution is insufficient to resolve this apex feature to the extent necessary to identify changes in the apex. Thus, the experiments we have performed cannot reveal the details of the cone apex.

2) We also note that the detailed structure of the apex region formed from detailed theoretical considerations is still an illusive problem. A model capable of predicting the detailed properties in the apex region as a function of field strength has still not been fully developed.

We therefore conclude that in the absence of either experimental or model data adopting a single value for radius of curvature is appropriate and can at least provide a method of highlighting underlying trends in the data.

The results of the field simulations, undertaken for each of the images captured for the cone structure, are summarized in Fig. 17. As we have seen, the different aspect ratio of the capillary and the emitter clearly contributes to the different voltages that are required to establish stable cone-jet mode operation. The linearity of the emitter length with voltage now is revealed to yield a notably different anticipated field strength characteristic from that for the capillary. It is also observed from the predictions of this simplified approach that as the cone length reduces the electric field is also lower for a given voltage, principally as a result of the increased distance between the cone tip and the counter electrode. This is of course counter to both electrospray observations and theoretical description that as the applied voltage is increased the cone length becomes shorter. Clearly, in our highly simplified approach, which does not include the electrohydrodynamics, the only way that the simulated field strength can increase, as the cone length reduces, is if there is a reduction in the radius of curvature of the cone tip. This model is therefore evidently not able to capture all of the crucial features of field mapping in the region of the cone.

However, to complete this analysis, we use these calculated values of field strength as the independent variable to replot the observed current data taking into account the apparent changes in the structure of the cone, as observed when the applied voltage is changed. This final comparison between observed current as a function of applied effective field strength is shown in Fig. 18 for the single flow rate of 55 nl/s. It is apparent from these data that the simplified model for field strength does not collapse the emitter and capillary data sets; indeed, the two data sets are now more discrepant than a direct comparison between the current-to-voltage characteristics seen in Fig. 14, where simple renormalization by aspect ratio was presented.

One feature we are clearly missing in this analysis is the way in which we have neglected the apex curvature region. Additional

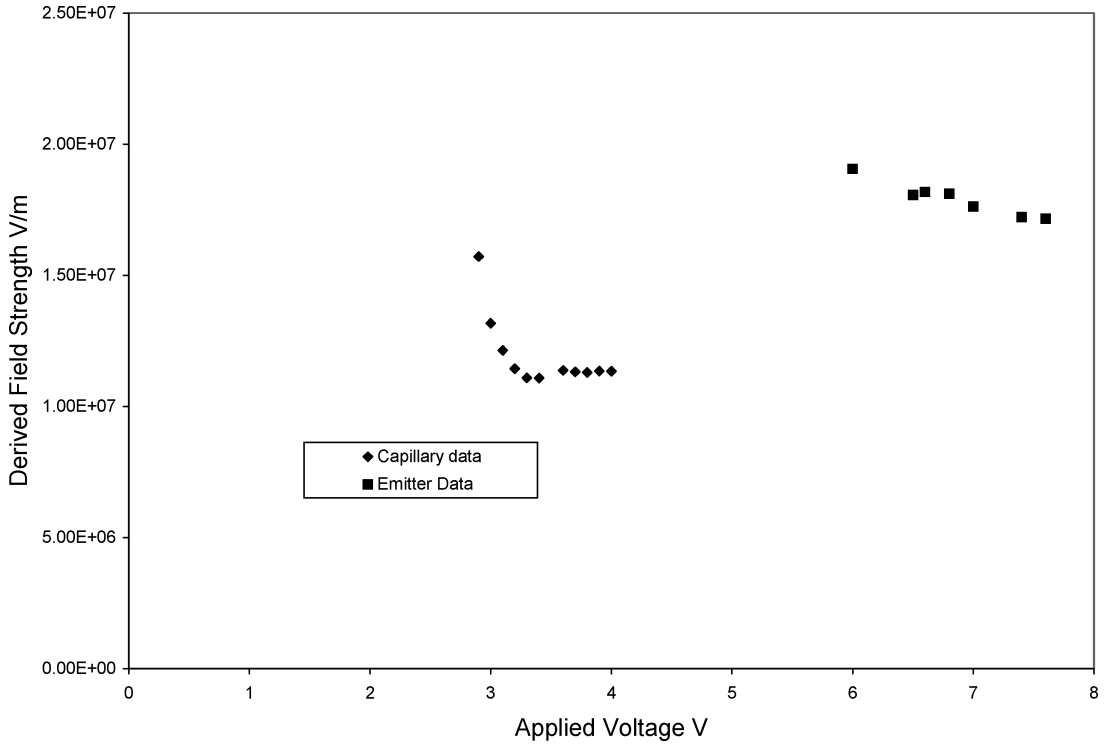

Fig. 17 Centerline field strength predicted using Simion7, for experimental configuration for both capillary and nano-emitter as a function of applied voltage, using the change in cone length observed in Fig. 15.

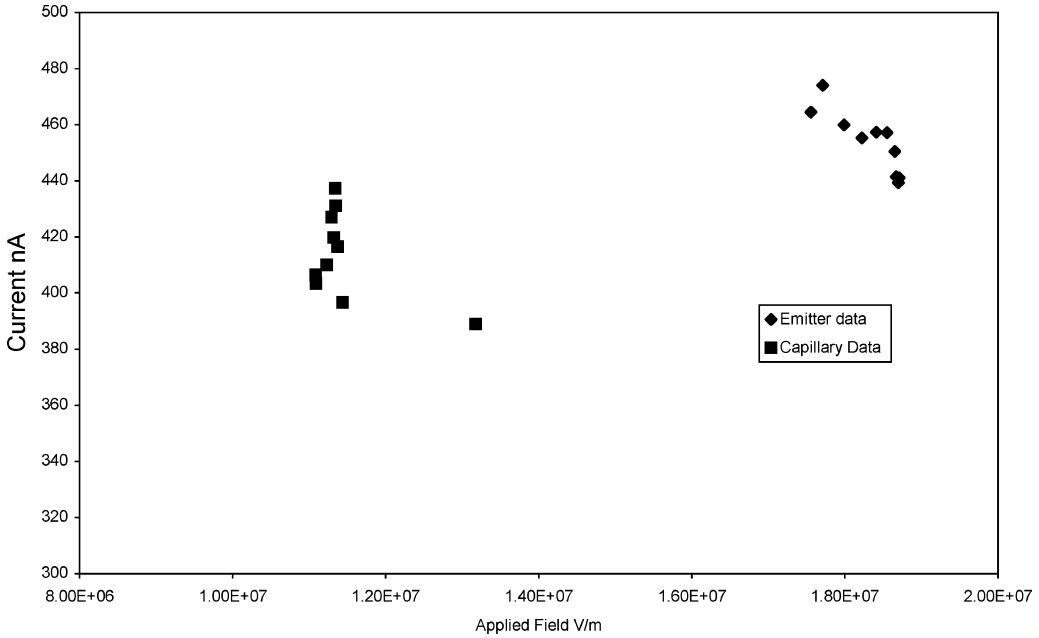

Fig. 18 Dependence of observed current to applied field strength for flow rate of 55 nl/s (see text for details).

simulations have been undertaken wherein the apex curvature is indeed reduced to evaluate this possible influence on field strength. From these it is apparent that the field will be enhanced by a factor of 3 to 4, even when only modest changes for this curvature are made. The observed applied voltage ratio between capillary data and the nano-emitter data required to achieve cone-jet mode spraying is significantly less than this factor. It is clear therefore that if a quantitative evaluation is to be undertaken to map current as a function of field strength in the vicinity of the apex region for the two different spray configurations either direct measurement of the cone apex structure or a more detailed model of both apex curvature and the jet structure itself is essential.

As we have seen, variation in applied voltage affects the cone shape in different ways for the capillary and emitter configurations. As a result, it would not be expected that the current-voltage gradient would necessarily be the same for the two sets of data, because the fields will be changing at different rates. It would be wrong therefore to conclude from the data presented that the observed difference in these gradients is significant. We have seen from the data that qualitatively the spray current obtained from the nano-emitter is similar to that from the stainless-steel emitter in these two cases,

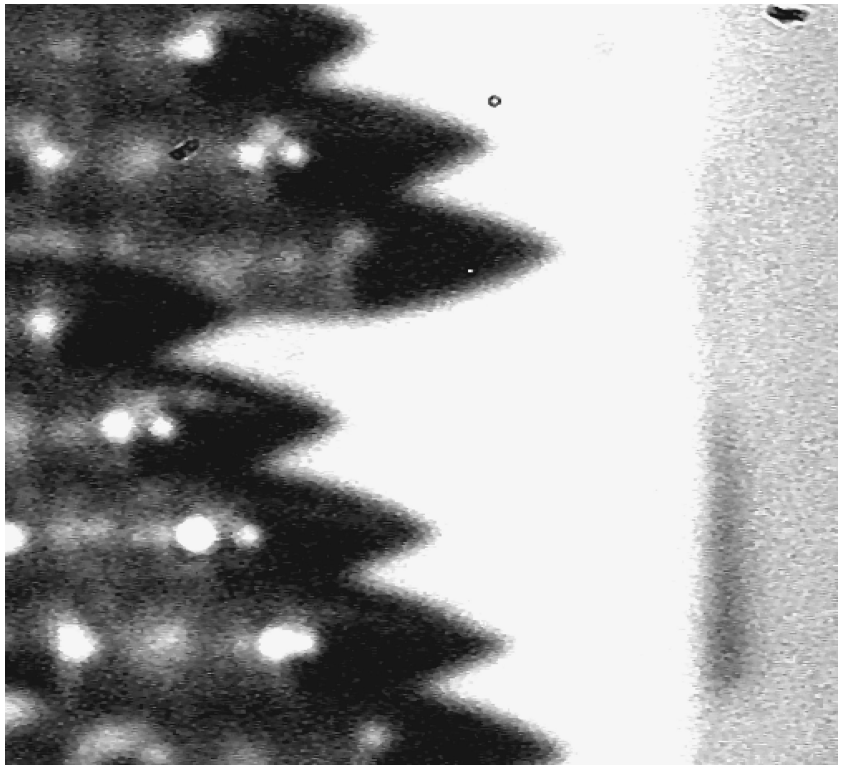

Fig. 19 High-resolution image of electrospray from a 19-element microfabricated nano-emitter array.

but there are quantitative differences, which at this stage we have been unable to resolve. We are not therefore able at this stage to definitively answer the question concerning the efficiency of nano-emitter electrospraying relative to stainless-steel capillary spraying.

Discussion

The results we have presented here have focused upon the electrospray properties from single nano-emitters, fabricated from silicon wafer material. We have also demonstrated that the fabrication processes we have adopted enable large area arrays of identical emitters to be produced. Although we are still evaluating the detailed properties of spraying from such arrays, the design concept we have adopted is capable of electrospraying from such arrays. In demonstration of this, Fig. 19 provides a high-resolution image of one part of an array of 19 emitters, each of outside diameter 175 μm, while electrospraying. It is therefore appropriate to consider the data we have obtained from a single emitter in the context of a full colloid thruster design.

The data we have obtained, as noted earlier, resulted from a liquid that we would not anticipate using in an operational thruster. The principal reason why this liquid is unsuited is that the specific impulse available at attainable acceleration potentials from onboard dc/dc converters would not be sufficiently high to be attractive and competitive with other propulsion systems, including bipropellant thrusters. However, even though we were not able to measure directly either the thrust or the specific impulse we can, using the data we acquired, provide indicative performance in the configuration tested.

From Fig. 11, and adopting 8 kV as a notional operating point for the thruster, we can identify that the charge-to-mass ratio q/m is a function of flow rate, with this value reducing with increasing flow rate, as expected. For the TEG/NaI solution the minimum stable flow rate is $\sim$1 nl/s (Ref. 8) with an anticipated q/m value of 74 C/kg. We note from Fig. 11 that at a flow rate of 54 nl/s this value for q/m has dropped to 5 C/kg; other results, not shown in Fig. 11, identify that at 10 nl/s the q/m value is 30 C/kg. This reveals the close coupling between flow rate and q/m. As a result, a colloid thruster design for a usable unit on a space vehicle will need to carefully consider the interaction between thrust and power for any specific application. However, referring to the data in Fig. 11, the range of I_{sp} attainable would be modest, having at 8 kV a value of 28 s. For a single emitter at the flow rates noted, the thrust would range from 17 to 48 μN. This further reinforces the observation that the test liquid here is unsuited to real spacecraft operation. The focus, however, in this paper is the viability of spraying from microfabricated components and in the identification of additional trends not apparent from spraying with conventional capillary systems.

In this regard we have noted for the first time that the spray efficiency, in terms of the current carried by the spray at a given flow rate, appears to be a function of the area available for the electrochemical reactions to take place. In this context the electrochemical reactions are those required to support the net charge separation that can take place at the solid/liquid boundary. Because thrust developed in a thruster is dependent upon the current carried, electrospray efficiency will affect propellant utilization for the thruster. Hence the electrochemical reactions are not only an essential element in the process of charge separation, which underpins the operation of a colloid thruster, but they are also responsible for how effectively a quantity of propellant can be used to deliver thrust. The results therefore demonstrate the need to define the geometric properties of the emitter because the ability to define an efficient emitter configuration is essential in the development of an effective colloid thruster design. This is a new and important observation and informs the appropriate route to the design of a thruster. It further illustrates that microfabrication techniques are most suitable for colloid thrusters, because it is possible to define the emitter structure in a precisely defined and repeatable method, a feature not easily available with individually fabricated conventional emitter arrays.

We also note that the microfabrication processing routes we have adopted result in the potential for simple approaches to the selection of coating materials for the emitter. This coating is required to provide a high conductive (equipotential) surface to the exposed outer surface of the emitter structure. In the data reported here we have

exclusively used copper/chromium coating because this material is simple to deposit on the emitters. We are however aware that this is not a suited material for a flight thruster because copper has a low activation potential. Indeed we have observed anodic dissolution at specific locations on the emitter, as a result of redox reactions. Further work we are undertaking is therefore identifying the appropriate methods for putting more stable coatings on the emitters, including platinum.

In our own design concept we have separated the function of overall flow rate control from the electrohydrodynamic element of flow control, wherein the electric stress imposed upon the fluid free surface solely dictates the range of flow rate available. Clearly we still require the flow rate to be in the stable regime for operation. Alternative designs have considered the flow control to be dominated by the electrohydrodynamics, and the flow rate resulting is close to minimum flow rate. Thus in Ref. 12 the hydraulic loss in the supply line, from reservoir to emitter exit, dictates the flow rate. Because the hydraulic loss identifies key geometric properties of diameter and length of the supply feed to the emitter itself, the available surface area for electrochemistry in this type of design is principally driven by concerns associated with fixing the flow rate rather than emitter electrochemical efficiency per se. In another design fluid wicking along a nano-structure provides fluid feed[15]; again in this design the resulting flow rate is fixed by the electric stress on the liquid.

Our results therefore identify an important aspect, namely, emitter geometry has a significant influence on thruster design.

Conclusions

The fabrication of a range of nano-emitters has been achieved. The processing routes adopted facilitate a large number of emitters to be manufactured per unit area. These arrays of emitters have the potential to provide a high thrust density from a colloid thruster, making them ideally suited to applications onboard both microsatellites and more conventional satellites.

Comparison between spray properties from a nano-emitter fabricated in silicon and conventional stainless-steel emitters has identified that the structure of the cone is rather different for similar flow rates, but this is principally associated with the changed electric field structure around the short nano-emitters relative to the long stainless-steel capillaries used in our comparative experiments. Although there do not appear to be major differences in the spray current for capillaries and emitters that have the same internal and external diameters, it has been shown that the detailed comparison is difficult because of the changing geometry of the cone structure.

We have also observed for the first time that the spray current is different at the same flow conditions when a comparison is made for near identical emitters but wherein different values of internal and external diameters are adopted. These differences suggest that the geometric specification for a nano-emitter is important and affects the efficiency of the electrospray process. There is a need to investigate further this dependence on electrospray efficiency if a colloid thruster having high propellant utilization is to be achieved.

References

[1]Bailey, A. G., *Electrostatic Spraying of Liquids*, Research Studies Press, Ltd., Taunton, England, U.K., 1988, pp. 171–176.

[2]Hendricks, C. D., "Charged Particle Experiments," *Journal of Colloid and Interface Science*, Vol. 17, 1962, pp. 249–259.

[3]Perel, J., Bates, T., Mahoney, J., Moore, R. D., and Yahiku, A. Y., "Research on a Charged Particle Bipolar Thrustor," AIAA Paper 67-728, 1967.

[4]Fearn, D., and Smith, P., "The Application of Ion Propulsion to Intelsat VII Class Spacecraft," AIAA Paper 89-2275, 1989.

[5]Marcuccio, S., Giannelli, S., and Andrenucci, M., "Attitude and Orbit Control of Satellite and Constellations with FEEP Thrusters," IEPC Paper 97-188, ERPS, Cleveland, OH, 1997.

[6]Kidd, P. W., and Shelton, K. H., "Life Test (4350 h) of an Advanced Colloid Thruster Module," AIAA Paper 73-1078, 1973.

[7]Fenn, J. B., Mann, M., Meng, C. K., Wang, S. K., and Whitehouse, C., "Electrospray Ionization for Mass Spectrometry of Large Biomolecules," *Science*, Vol. 246, 1989, pp. 64–71.

[8]Fernandez de la Mora, J., and Loscertales, J. G., "Current Emitted by Highly Conducting Taylor Cones," *Journal of Fluid Mechanics*, Vol. 260, 1994, pp. 155–184.

[9]Hruby, V., Gamero-Castano, M., Falkos, P., and Shenoy, S., "Micro Newton Colloid Thruster System," IEPC-01-281, ERPS, Cleveland, OH, 2001.

[10]Zeleny, J., "Instability of Electrified Liquid Surfaces," *Physical Review*, Vol. 10, 1917, pp. 1–6.

[11]Taylor, G. I., "Disintegration of Water Drops in an Electric Field," *Proceedings of the Royal Society of London*, Vol. A280, 1964, pp. 383–397.

[12]Martinez-Sanchez, M., Fernandez de la Mora, J., Hruby, V., Gamero-Castano, M., and Khayms, V., "Research on Colloid Thrusters," IEPC-99-014, ERPS, Cleveland, OH, 1999, pp. 93–100.

[13]Pranajaya, F., and Cappelli, M., "Performance Studies of a Colloid Thruster System," IEPC Paper 01-284, ERPS, Cleveland, OH, Oct. 2001.

[14]Velasquez, L. F., and Martinez-Sanchez, M., "A Micro-Fabricated Colloid Thruster Array," AIAA Paper 2002-3810, July 2002.

[15]Velasquez, L. F., Carretero, J. A., Ankinwande, A. I., and Martinez-Sanchez, M., "The Concept and Development of a Micro-Fabricated Colloid Thruster Array," AIAA Paper 2003-4850, July 2003.

[16]Paine, M. D., "A Micro-Fabricated Colloid Microthruster: High Voltage Electrostatic Fields on a MEMS Device," Ph.D. Dissertation, Dept. of Aeronautics and Astronautics, Univ. of Southampton, England, U.K., April 2003.

[17]Stark, J., Kent, B., Stevens, R., Sandford, M., Alexander, M., Smith, K., and Paine, M., "Colloid Propulsion—a Re-evaluation, with an Integrated Design," AIAA Paper 2003-4851, July 2003.

[18]Stark, J., Smith, K., and Robertson, S., "High Accuracy Measurements in Electrospray Source Relevant to Colloid Thrusters," AIAA Paper 2003-4847, July 2003.

[19]Ganan-Calvo, A. M., Davila, J., and Barrero, A., "Current and Droplet Size in the Electrospraying of Liquids. Scaling Laws," *Journal of Aerosol Sciences*, Vol. 28, 1997, pp. 249–275.

[20]Smith, D. P., "The Electrohydrodynamic Atomization of Liquids," *IEEE Transactions on Industry Applications*, Vol. IA-122, May/June 1986, pp. 527–535.

[21]Chen, D., Pui, D. Y. H., and Kaufman, S., "Electrospraying of Conducting Liquids for Monodisperse Aerosol Generation in the 4 nm to 1.8 μ Diameter Range," *Journal of Aerosol Sciences*, Vol. 26, 1995, pp. 963–977.

[22]Gamero-Castano, M., and Hruby, V., "Electric Measurements of Charged Sprays Emitted by Cone-Jets," *Journal of Fluid Mechanics*, Vol. 459, 2002, pp. 245–276.

I. Boyd
Associate Editor